Journal of the American College of Cardiology
© 2011 by the American College of Cardiology Foundation
Published by Elsevier Inc.

Vol. 58, No. 24, 2011
ISSN 0735-1097/$36.00
doi:10.1016/j.jacc.2011.09.017

PRE-CLINICAL RESEARCH

In Vivo Characterization of a New Abdominal Aortic Aneurysm Mouse Model With Conventional and Molecular Magnetic Resonance Imaging

Ahmed Klink,* Joeri Heynens,† Beatriz Herranz, PhD,*‡ Mark E. Lobatto, MD,*§ Teresa Arias, PhD,*‡ Honorius M. H. F. Sanders, PhD,† Gustav J. Strijkers, PhD,† Maarten Merkx, PhD,† Klaas Nicolay, PhD,† Valentin Fuster, MD, PhD,‡‖ Alain Tedgui, PhD,¶ Ziad Mallat, MD, PhD,# Willem J. M. Mulder, PhD,* Zahi A. Fayad, PhD*‖

New York, New York; Eindhoven and Amsterdam, the Netherlands; Madrid, Spain; Paris, France; and Cambridge, United Kingdom

Objectives The goal of this study was to use noninvasive conventional and molecular magnetic resonance imaging (MRI) to detect and characterize abdominal aortic aneurysms (AAAs) in vivo.

Background Collagen is an essential constituent of aneurysms. Noninvasive MRI of collagen may represent an opportunity to help detect and better characterize AAAs and initiate intervention.

Methods We used an AAA C57BL/6 mouse model in which a combination of angiotensin II infusion and transforming growth factor–β neutralization results in AAA formation with incidence of aortic rupture. High-resolution, multisequence MRI was performed to characterize the temporal progression of an AAA. To allow molecular MRI of collagen, paramagnetic/fluorescent micellar nanoparticles functionalized with a collagen-binding protein (CNA-35) were intravenously administered. In vivo imaging results were corroborated with immunohistochemistry and confocal fluorescence microscopy.

Results High-resolution, multisequence MRI allowed the visualization of the primary fibrotic response in the aortic wall. As the aneurysm progressed, the formation of a secondary channel or dissection was detected. Further analysis revealed a dramatic increase of the aortic diameter. Injection of CNA-35 micelles resulted in a significantly higher magnetic resonance signal enhancement in the aneurysmal wall compared with nonspecific micelles. Histological studies revealed the presence of collagen in regions of magnetic resonance signal enhancement, and confocal microscopy proved the precise co-localization of CNA-35 micelles with type I collagen. In addition, in a proof-of-concept experiment, we reported the potential of CNA-35 micelles to discriminate between stable AAA lesions and aneurysms that were likely to rapidly progress or rupture.

Conclusions High-resolution, multisequence MRI allowed longitudinal monitoring of AAA progression while the presence of collagen was visualized by nanoparticle-enhanced MRI. (J Am Coll Cardiol 2011;58:2522–30) © 2011 by the American College of Cardiology Foundation

Abdominal aortic aneurysms (AAAs) are permanent dilations of the abdominal aorta that exceed the normal diameter by >50% and which present a life-threatening degenerative disease. They occur in 5% to 9% of the population

See page 2531

From the *Translational and Molecular Imaging Institute, Mount Sinai School of Medicine, New York, New York; †Eindhoven University of Technology, Department of Biomedical Engineering, Laboratory of Chemical Biology, Eindhoven, the Netherlands; ‡Department of Epidemiology, Atherothrombosis and Imaging, Centro Nacional de Investigaciones Cardiovasculares (CNIC), Madrid, Spain; §Department of Vascular Medicine, Amsterdam Medical Center, Amsterdam, the Netherlands; ‖The Zena and Michael A. Wiener Cardiovascular Institute and the Marie-Josee and Henry R. Kravis Center for Cardiovascular Health, Mount Sinai Medical Center, New York, New York; ¶Paris Cardiovascular Research Center, Georges Pompidou European Hospital, Paris, France; and the #Department of Medicine, University of Cambridge, Cambridge, United Kingdom. This study was funded by the Netherlands Heart Foundation project number 2009SB006, the collaborative project ATHIM (Atherothrombosis Molecular Imaging), NIH/NHLBI R01HL070121, and NIH/NIBIB R01EB009638 (Dr. Fayad). All other authors have reported that they have no relationships relevant to the contents of this paper to disclose.

Manuscript received June 30, 2011; revised manuscript received August 17, 2011, accepted September 5, 2011.

over the age of 65 years and are the tenth leading cause of death in western countries (1). AAA progression is characterized by a long period of asymptomatic growth of the abdominal aorta. Once it reaches 5.5 cm, there is an increased chance of rupture, with a mortality rate >80%. Surgery and endovascular aortic repair (EVAR) are currently the only interventions for patients diagnosed with AAA. These procedures are costly and associated with high morbidity and mortality rates (2). Generally, surgery or EVAR is recommended when the AAA reaches a size of 55 mm or if the expansion rate is >1 cm/year (2). Although currently the best predictor of aneurysm expansion is the baseline size at diagnosis (3), the prognosis remains complex due to the nonlinearity and unpredictability of expansion rates (4). More specific prognostic predictors would offer the chance to better select intervention strategies for individual patients.

Different animal models have been developed in the past several years to improve the understanding of AAA pathophysiology. Recently, Wang et al. (5) introduced a model in which a combination of angiotensin II (Ang II) and anti-transforming growth factor (TGF)-β administered to C57BL/6 wild-type mice leads to AAA formation and the occurrence of fatal AAA rupture as high as 80%. Currently, this is the only animal model that displays such a relevant rate of AAA rupture, thereby enabling monitoring of the mechanisms at play in this fatal process.

The degradation of the extracellular matrix (ECM) in the medial wall is key to the formation, progression, and rupture of AAAs (6). Particularly, the turnover of collagen, an essential component of the ECM, is known to be responsible for the remodeling that occurs in the adventitia. Studies indicate that perturbations in collagen microarchitecture and networks, probably as a result of collagen degradation and inappropriate collagen deposition, may alter vessel wall response to mechanical load and lead to vessel wall failure (7). Therefore, imaging collagen in AAAs might provide valuable information about the state of aneurysm development and the identification of AAAs prone to severely progress or rupture.

In the current work, we first explored the use of multisequence, high-field magnetic resonance imaging (MRI) to characterize the development of AAAs in the aforementioned model. We then applied recently developed fluorescent/paramagnetic nanoparticles (8), functionalized with a collagen-specific protein (CNA-35) (9–13), to identify the presence of collagen in the aneurysmal wall using molecular MRI. Finally, in a proof-of-concept experiment, we studied the potential of CNA-35 micelles to discriminate between stable AAAs and aneurysms prone to progress and eventually rupture.

Methods

Animal model. All the procedures were approved by the Mount Sinai School of Medicine Institutional Animal Care and Use Committee. C57BL/6J male mice (The Jackson Laboratory, Bar Harbor, Maine) between the ages of 8 and 12 weeks were used. As described in more detail by Wang et al. (5), AAAs were induced in wild-type mice by continuous infusion of Ang II at 1,000 ng/kg/min for a maximum of 28 days, along with systemic neutralization of TGF-β. Briefly, animals were anesthetized with isoflurane (4% induction, 1.5% maintenance), and mini-pumps (Alzet, model 2004 DURECT Corporation, Cupertino, California) containing 200 μl of Ang II were implanted subcutaneously. To achieve systemic neutralization of TGF-β, intraperitoneal injections of an anti–TGF-β antibody (dose: 20 mg/kg) were performed every other day, which results in AAA formation in the suprarenal region of the aorta.

Abbreviations and Acronyms

- **AAA** = abdominal aortic aneurysm
- **AngII** = angiotensin II
- **CLSM** = confocal laser scanning microscopy
- **CME** = combined Masson elastin
- **ECM** = extracellular matrix
- **EVAR** = endovascular aortic repair
- **MR** = magnetic resonance
- **MRI** = magnetic resonance imaging
- **NIRF** = near-infrared fluorescence
- **%NSE** = normalized percentage signal enhancement
- **PDW** = proton density–weighted
- **T1W** = T1-weighted
- **T2W** = T2-weighted
- **TGF** = tumor growth factor

Multisequence in vivo MRI of AAA progression. AAAs were induced in a group of mice as described above (n = 3). MRI scanning was performed using a 9.4-T, small-animal, vertical bore MRI scanner (Bruker BioSpec, Bruker, Germany). Each animal was placed in the center of a whole-body coil (35-mm inner diameter), under continuous isoflurane anesthesia, which was positioned in the scanner. The animals were connected to a respiratory rate monitor, and the flow of anesthetic gas was constantly regulated to maintain a breathing rate of 60 breaths/min. Baseline MRI scanning was followed by scans every other day until sacrifice. Each scan session started with a pilot scan with 3 orthogonal slices, followed by high-resolution, black-blood T1-weighted (T1W), T2-weighted (T2W), and proton density–weighted (PDW) spin echo imaging, of which the exact parameters are reported in the online version of this paper. The suprarenal region of the aorta encompassing 22 mm immediately superior to the right renal artery was imaged. Subsequently, a time-of-flight angiography sequence was used to visualize the blood flow and generate a 3-dimensional reconstruction of the aorta to allow visualization of vessel dilation.

Molecular MRI of collagen. AAAs were induced in wild-type mice (n = 10) according to the aforementioned protocol. The presence of an aneurysm was assessed using magnetic resonance (MR) angiography. CNA-35 micelles or the mutant Y175K CNA-35 micelles (12) (dose: 50 μmol Gd/kg) were injected in the tail vein of the animals (n = 5 for each group). The mice were imaged pre- and 32 hours' post-injection to allow proper clearance of the micelles from the circulating blood, using a T1W spin echo sequence, with the same parameters as used for the multispectral imaging group (Online Appendix). To ensure that AAA remodeling remained minimal between pre- and

post-imaging sessions, the injections of anti–TGF-β antibody were terminated before the imaging sessions. Animals that received subcutaneous infusion and intraperitoneal injections of saline were injected with CNA-35 micelles and used as controls (n = 4). In addition, the half-life of CNA-35 micelles was investigated by collecting blood samples at different time points over a period of 24 h. The blood samples were imaged on the IVIS optical system (Calliper Life Sciences, Inc., Hopkinton, Massachusetts), and photon counts were measured to determine the half-life.

Predictive value of (molecular) MRI for the assessment of experimental AAA. AAA were induced in C57BL/6 mice (n = 8) as described here (10 mg/kg). To study whether CNA-35 micelles-enhanced molecular MRI can discriminate between stable AAA lesions and aneurysms that are prone to severely progress or rupture, animals underwent MR imaging after intravenous administration of CNA-35 micelles at days 5 and 15 after the onset of AAA. These animals were monitored for death or survival, whereas aneurysm severity (stage I to stage IV) was assessed by looking at aneurysm morphology as previously described (14). Mice that suffered from ruptured aneurysms were classified as stage IV.

Image analysis and statistics. Pre- and post-MR images were analyzed using OsiriX DICOM Viewer (Geneva, Switzerland). Each slice was co-registered using the spinal cord as a landmark. AAAs were identified on the pre-injection images. A region of interest was drawn around the aneurysmal wall, and the average signal intensity was measured (I_{wall}) over 10 slices throughout the aneurysm. In addition, regions of interest were also drawn in the surrounding muscle as well as in the noise, and the average signal intensity and SD of the noise were measured, respectively (I_{muscle}, σ_{noise}). Signal-to-noise ratios were calculated for the wall and the muscle ($SNR_{Wall} = I_{Wall}/\sigma_{Noise}$, $SNR_{Muscle} = I_{Muscle}/\sigma_{Noise}$). The contrast-to-noise ratio was calculated ($CNR_{WM} = SNR_{Wall}/SNR_{Muscle}$) and further normalized to the pre-injection values ($CNR_{Norm} = CNR_{WM\ post}/CNR_{WM\ pre}$). Finally, the normalized percentage signal enhancement (%NSE) was determined as $\%NSE = (CNR_{Norm} - 1) \times 100$. The data are presented as mean ± SD.

One-way and 2-way analysis of variance (ANOVA) tests were performed to determine statistical significance. A post-hoc Tukey test was performed to compare each of the 3 groups injected with CNA-35 micelles or mutant CNA-35 micelles. A Bonferroni post-hoc test was performed to compare the %NSE of stages II, III, and IV aneurysms at days 5 and 15 of AAA development. A p value <0.05 was considered statistically significant. Statistical analysis was performed using PRISM (GraphPad Software, La Jolla, California).

Immunohistochemistry and confocal microscopy. Animals were sacrificed by an isoflurane overdose. Transcardiac perfusions through the left ventricle were conducted with saline and paraformaldehyde (4%). The suprarenal aorta was excised, collected in optimum cutting temperature medium (OCT), and frozen for further histological examination. Combined Masson elastin (CME) staining was performed to stain for collagen and elastin fibers. In addition, type I collagen and macrophage CD68 staining was performed using a primary rabbit anti-mouse type I collagen antibody and a primary rat anti-mouse CD68 antibody, respectively (Santa Cruz Biotechnology, Inc., Santa Cruz, California); the primary antibodies were detected using appropriate secondary antibodies coupled to an Alexa 647 fluorophore. For each animal, 10 representative sections were chosen, fixed in 4% paraformaldehyde, and washed twice in phosphate-buffered saline. The sections were blocked with 2% goat serum in phosphate-buffered saline for 20 min at room temperature. After blocking, the sections were incubated with the type I collagen primary antibody or CD68 primary antibody (1:100 dilution) for an hour. After washing with phosphate-buffered saline, the secondary antibody was added for 30 min. Finally, the autofluorescence of the tissue was reduced using copper sulfate, and sections were mounted with DAPI-containing VECTASHIELD mounting medium (Vector Laboratories Inc, Burlingame, California) and sealed with coverslips, shielded from light, and kept at 4°C until confocal laser scanning microscopy (CLSM) was performed within 48 h. Sections incubated with the secondary antibody only were used as negative controls. CLSM imaging was performed with a Leica Sp5DM microscope (Leica Microsystems, Wetzlar, Germany). Adjacent sections were stained for type I collagen and macrophages to study their respective localization with regard to the rhodamine-labeled CNA-35 micelles.

Results

Characterization and in vitro binding experiments. The synthesis and a schematic of the paramagnetic micelles are included in the Online Appendix (Online Fig. 1A). The size of the micelles before conjugation was 14 ± 1.5 nm, whereas the CNA-35 and mutant CNA-35–coupled micelles had a mean size of 25 ± 3 nm. Phosphate determination and protein determination yielded a lipid:protein ratio of approximately 50:1, corresponding to approximately 2 proteins per micelle. The ionic relaxivity, a measure of MRI contrast–generating potency (15), of bare, CNA-35, or mutant CNA-35–conjugated micelles was 12 $mM^{-1}s^{-1}$.

CNA-35 is a natural collagen-binding protein that has been shown to have affinity for collagen fibers (11). Indeed, collagen fibers contain a high density of binding sites with both high and low affinity for the CNA-35 protein, resulting in an average constant dissociation value of 500 nm (11). Our in vitro binding experiment (described in the Online paper) corroborated these previously published findings (11). We observed an apparent binding of the CNA-35 micelles to collagen after extensive washing, whereas little binding occurred for mutant CNA-35 or unconjugated micelles (Online Fig. 1B). A second in vitro experiment was performed to further confirm these findings and to investigate the collagen binding of Cy5.5-labeled CNA-35 mi-

celles with near-infrared fluorescence (NIRF) imaging using the IVIS optical imaging system. Similar to the plate reader studies, we found a clear binding of the CNA-35 micelles to collagen (Online Fig. 1C). Finally, the blood circulation half-life of the CNA-35 micelles in male C57BL/6 mice (n = 2) was determined to be 4.3 h.

Multisequence in vivo imaging of AAA progression. AAAs were induced in male C57BL/6 mice through continuous infusion of Ang II and administration of anti–TGF-β every other day. The abdominal region of these mice was imaged using high-resolution, multisequence MRI to monitor the temporal progression of the AAA at the anatomical level. T1W, T2W, and PDW MRI, as well as MRI angiography, were performed. Multisequence MRI allowed the visualization of the primary fibrotic response in the aortic wall at day 3. It also revealed luminal stenosis and medial rupture, with blood infiltrating the adventitial tissue 6 days after AAA induction (Figs. 1A to 1C). At day 8, the adventitia appeared to be extensively destructed, with the formation of a double channel clearly visible on different sequences. The 3-dimensional reconstruction resulting from the time-of-flight angiography confirmed the aortic dilation and the presence of blood infiltrating the adventitial tissue (Fig. 1D, arrow). Additional analysis revealed a dramatic increase in the diameter of the aorta, reaching 50% growth at day 5 and up to a 150% growth on day 15 (Fig. 1F). To corroborate the in vivo findings, immunohistological examination of the aortas was performed at the animals' death. The results confirmed the presence of AAAs and allowed the precise validation of several features of vessel wall remodeling observed by using in vivo MRI. An extreme degradation of the ECM was observed due to massive destruction of adventitial collagen. Only a thin cap remained visible on the outer edge of the aneurysmal wall, preventing the vessel from rupturing. Intense degradation of the elastin fibers as well as the complete rupture of the medial layer of the aorta was clearly identified (Fig. 1E, arrow). Due to the rupture, blood originating from the aortic lumen was able to infiltrate the adventitia, thereby forming a secondary lumen referred to as false channel or dissection (Fig. 1E). The resulting increase of the aortic diameter was visibly noted.

In vivo molecular imaging of collagen. Although high-resolution, multisequence MRI allows the characterization

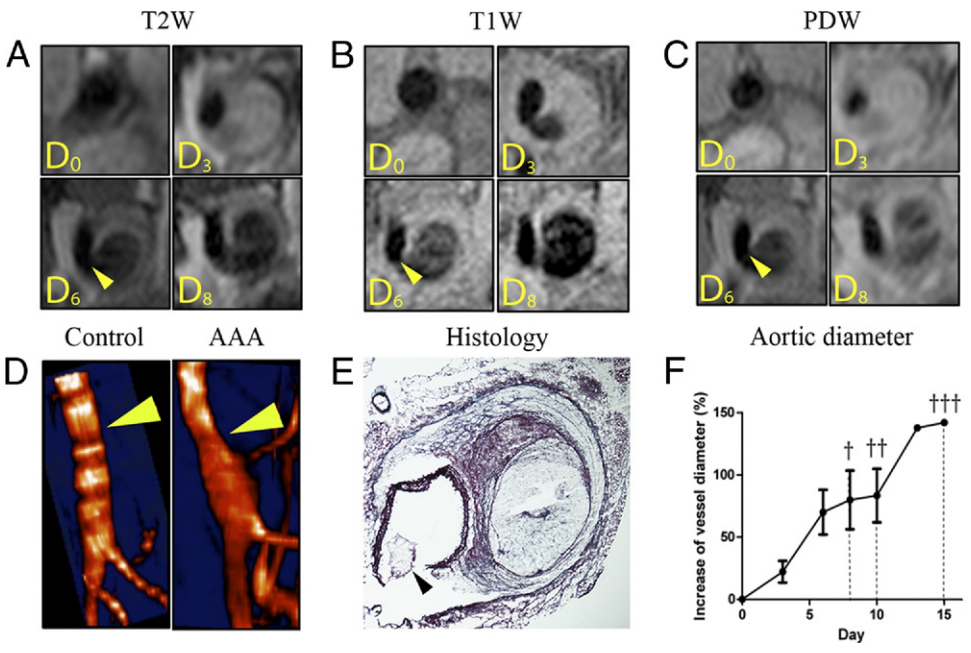

Figure 1 **High-Resolution, Multisequence MRI of AAA Progression Over the Course of 8 Days**

(A) T2-weighted (T2W) black-blood imaging of abdominal aortic aneurysm (AAA) progression over the course of 8 days. The primary fibrotic response and luminal stenosis is visualized at 3 days after AAA induction in the upper-right corner. At 6 days, the medial rupture with blood infiltrating the adventitial tissue is visible **(arrow)**. At day 8, the formation of a second channel is clearly visible in the bottom-right corner. **(B)** T1-weighted (T1W) black-blood imaging of AAA progression over the course of 8 days. Medial rupture is visible here as soon as 3 days after the induction of AAA in the upper-right corner. The formation of a false channel with probable disturbed blood flow extravasating in the adventitia is visualized at day 6. At day 8, the formation of the false channel is clearly visible. **(C)** Proton density–weighted (PDW) black-blood imaging of AAA progression over the course of 8 days. The primary fibrotic response, the medial rupture, and false channel formation were all observed, respectively, at days 3, 6, and 8 after AAA induction. **(D)** Three-dimensional magnetic resonance (MR) time-of-flight angiography of a healthy aorta and AAA. Aortic dilation due to medial rupture and blood infiltration in the adventitia is visible **(arrow)**. **(E)** Histology with combined Masson elastin staining confirmed the presence of the medial rupture and degradation of the elastic lamina as well as the extreme remodeling of the adventitia and formation of a false channel. **(F)** The increase of aortic diameter was averaged from the 3 sequences (T1W, T2W, and PDW) at each imaging time point and plotted. A 50% increase, which is the minimum size to define the presence of AAA, was reached 5 days after AAA induction. The days of animals' death from AAA rupture were noted and are marked with a **cross**.

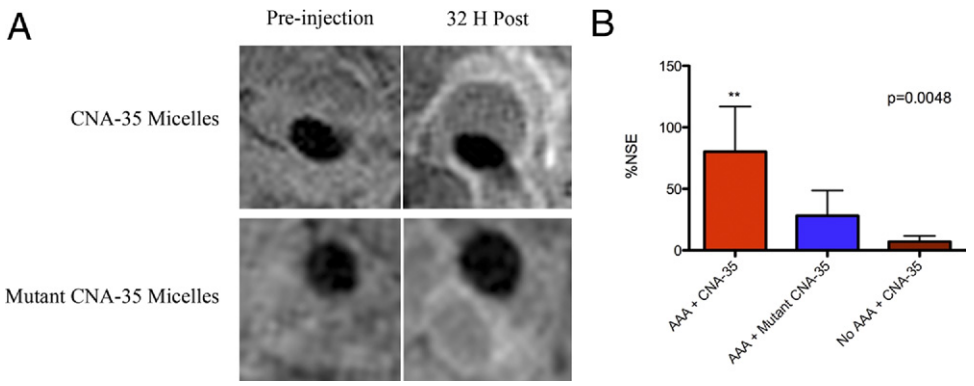

Figure 2 In Vivo MR Molecular Imaging of Collagen

(A) Representative images of animals bearing abdominal aortic aneurysms (AAAs) and injected with CNA-35 micelles or mutant CNA-35 micelles. The injection of CNA-35 micelles caused an important signal enhancement in the aneurysmal wall compared with mutant CNA-35 micelles. The normalized signal enhancement percentage (%NSE) deriving from the aneurysmal wall was calculated in both groups and is plotted in **(B)**. The data analysis is presented as mean ± SD. CNA-35 micelles injected in animals with AAAs caused a significant magnetic resonance (MR) signal enhancement compared with mutant CNA-35 micelles and CNA-35 micelles injected in healthy animals. *$p < 0.01$.

of AAA progression on an anatomical level, it does not provide any information on the underlying molecular biological processes. Therefore, we decided to evaluate the presence of collagen in the same mouse model because it represents a key constituent of aneurysms. To that end, collagen-specific CNA-35 micelles were synthesized and injected for nanoparticle-enhanced MR imaging. Before the injection of micelles, the presence of aneurysms was evaluated using MR angiography. T1W MR images were then acquired before and 32 hours after injection of CNA-35 or mutant CNA-35 micelles. In mice injected with CNA-35 micelles, a clear signal enhancement in the aneurysmal region was observed (Fig. 2A), whereas a significantly lower signal enhancement was visible after the injection of mutant CNA-35 micelles. As shown in Figure 2B, data analysis of the MR images revealed an 80.15 ± 37% increase in %NSE after injection of CNA-35 micelles compared with a 30.90% ± 19% increase after the injection of mutant CNA-35 micelles ($n = 5$; $p = 0.0048$, 1-way ANOVA test; $p < 0.05$, post-hoc Tukey test). No enhancement was observed in healthy animals injected with CNA-35 micelles.

Examination of the corresponding histological slices stained with CME revealed an advanced degree of adventitial destruction with the presence of collagen in the areas of MR signal enhancement (Figs. 3B, 3C, 3F, and 3G). Importantly, further examination by confocal microscopy demonstrated the co-localization of the CNA-35 micelles

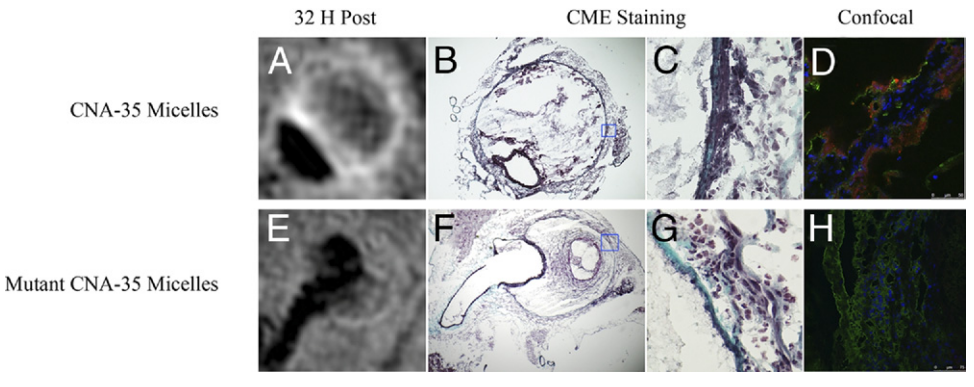

Figure 3 Correlation of In Vivo MRI Findings With Histological Sections and Confocal Fluorescence Microscopy

(A) Typical image of an aneurysm after the injection of CNA-35 micelles showing magnetic resonance signal enhancement in the aneurysmal wall. **(B)** Corresponding histological section stained with combined Masson elastin (CME) showing the presence of collagen in the areas of signal enhancement. **(C)** Represents a 40× magnification of the remodeled adventitia with collagen stained in blue. **(D)** Representative image of fluorescent confocal microscopy showing the precise co-localization of CNA-35 micelles **(red)** with collagen I staining **(green)**. **(E)** Typical image of an aneurysm after the injection of mutant CNA-35 micelles showing no significant magnetic resonance signal enhancement in the aneurysmal wall. **(F)** Corresponding histological section confirming the presence of collagen stained in blue on the 40× magnification shown in **(G)**. **(H)** Representative image of fluorescent confocal microscopy of animals injected with mutant CNA-35 micelles showing no micelles in the areas of collagen staining **(green)**. MRI = magnetic resonance imaging.

(red) with collagen-I (green) in the adventitia (Fig. 3D). In animals injected with mutant CNA-35 micelles, the fluorescent signal originating from the micelles was found to be nearly nonexistent in the regions that stained positively for type I collagen (Fig. 3H). In addition, CLSM images of macrophage stained with a CD68 antibody revealed no association between macrophages and CNA-35 or mutant CNA-35 micelles (data not shown). It is noteworthy that mutant CNA-35 micelles were not associated with any specific biological structures. In addition, the collagen MR signal enhancement pattern observed in different animals allowed differentiation between collagen-rich and collagen-poor lesions as observed on corresponding CME stains (Fig. 4).

Ex vivo fluorescence imaging. To corroborate the CNA-35 micelles-enhanced in vivo MRI results and to investigate their spatial distribution in the aorta, Cy5.5-labeled micelles were injected in mice after AAA development as well as in healthy animals. NIRF imaging, a so-called hotspot imaging technique (16), allows the visualization of the Cy5.5-labeled micelles with high sensitivity in intact aortas (17,18). Mice were sacrificed 32 hours post-injection, and the excised aortas were imaged with NIRF imaging. Cy5.5-labeled CNA-35 micelles were clearly observed in the AAA region (Online Fig. 2). In comparison, healthy animals and noninjected AAA animals marginally displayed fluorescent signals, further supporting the specific binding of CNA-35 micelles in the aneurysmal region.

Predictive value of (molecular) MRI for the assessment of experimental AAA. As described here, the injection of CNA-35 micelles allowed the discrimination between collagen-poor and collagen-rich lesions (Fig. 4). It has been shown in the literature that low levels of collagen are associated with AAA progression and ultimately rupture (7). Hence, we hypothesized that CNA-35 micelles have the potential to discriminate between stable AAA lesions and aneurysms that are prone to progress or rupture. We imaged CNA-35–injected animals at days 5 and 15 of AAA development and subsequently monitored them for survival. On death or sacrifice, the aneurysm severity was evaluated by looking at the aneurysm morphology as previously described (14). Administration of anti–TGF-β in Ang II–infused mice led to mortality from aneurysm rupture (stage IV) in 3 mice, whereas the remaining 5 animals survived bearing stage II and III AAAs. All the main features of human aneurysms ranging from the fibrotic response around the vessel wall to signs of medial dissection and formation of a secondary channel were observed.

As shown in Figure 5, animals that were morphologically classified with stage II aneurysms displayed marked enhancement after CNA-35 administration at days 5 and 15 of aneurysmal development, suggesting a collagen-rich response of the aortic wall. These lesions were stable, as no aortic dissection and medial rupture were observed, and the

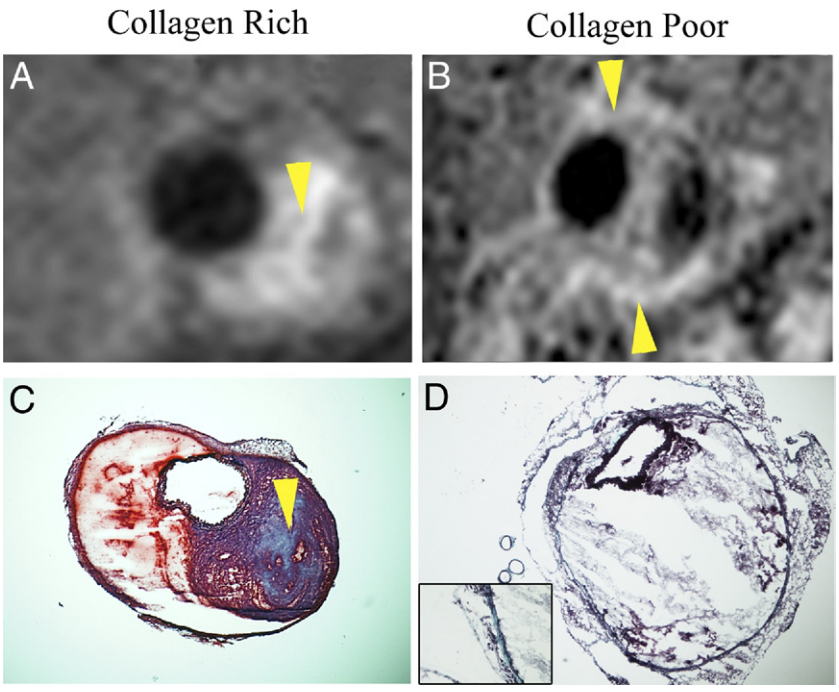

Figure 4 Spatial Correlation Between the Pattern of MR Signal Enhancement and the Collagen Content Observed by Using Histology

(A) Representative image of a collagen-rich aneurysmal lesion after the injection of CNA-35 micelles. The high collagen content was confirmed to be present in the area of magnetic resonance (MR) signal enhancement **(arrows)** by combined Masson elastin histological staining as shown in **C**. **(B)** Representative image of a collagen-poor aneurysmal lesion after the injection of CNA-35 micelles. A thin layer of collagen was identified by combined Masson elastin staining in the region of MR signal enhancement **(arrows)** as shown in **D**.

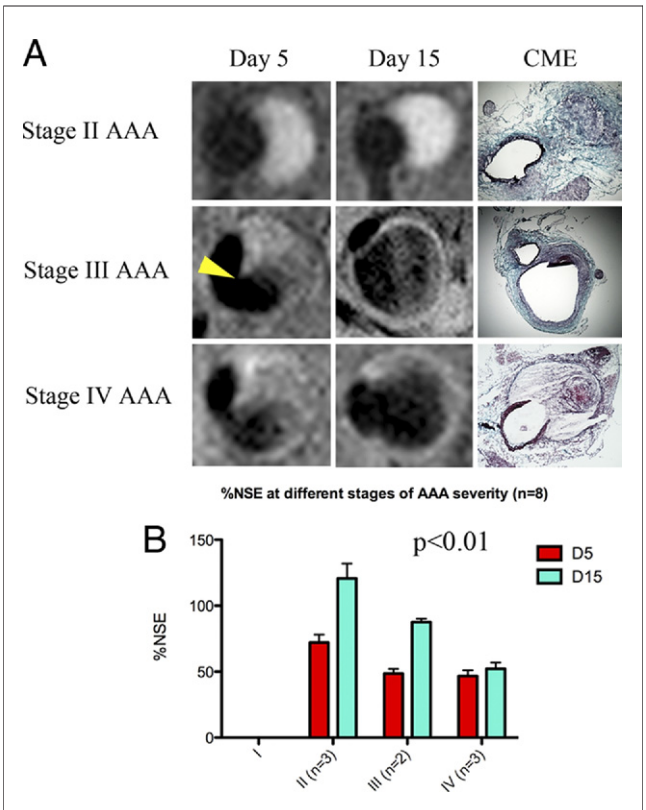

Figure 5 **CNA-35–Enhanced MR Imaging of AAAs of Increasing Severity at Early and Late Stage of Development and Complications**

(A) Typical images of stage II, III, and IV abdominal aortic aneurysms (AAAs) obtained after CNA-35 injection at day 5 and day 15 of AAA development. Corresponding histological sections stained with combined Masson elastin (CME) are shown in the third column. **(B)** Quantification of aneurysm severity (increasing from stage I to IV) and normalized signal enhancement percentage (%NSE) relative to CNA-35 injection in a group of mice (n = 8).

animal survived the 28-day period of Ang II + anti–TGF-β administration. In contrast, all the mice retrospectively classified with stage III and IV aneurysms (n = 5) exhibited a dissection of the media at day 5 (Fig. 5A, arrow) and showed a marked decrease of approximately 30% in %NSE in both groups relative to stage II AAAs (48.50 ± 4.950 vs. 72.01 ± 10.47 [$p > 0.05$] and 46.68 ± 7.652 vs. 72.01 ± 10.47 [$p > 0.05$], respectively) (Fig. 5B). Imaging at day 15 showed a critical progression of AAA development with an extensive remodeling of the vessel wall and presence of a secondary channel. Ruptured stage IV aneurysms showed little signal enhancement after CNA-35 injection, suggesting a lower collagen content as opposed to nonruptured stage II and III aneurysms (52.13 ± 8.408% vs. 120.7 ± 19.49% [$p < 0.001$] and 52.13 ± 8.408% vs. 87.51 ± 3.521% [$p < 0.05$], respectively) (Fig. 5B). Consistent with this hypothesis, histological examination on the death of the animals at days 19, 22, and 23 revealed substantial collagen degradation in fatal aneurysms compared with viable stage II and III AAAs. A 2-way ANOVA test revealed that both factors (stage of aneurysm and time) significantly alter %NSE ($p = 0.0027$ and $p = 0.0024$, respectively) and that there is a significant interaction between the 2 factors ($p = 0.0407$). These findings show a potential for CNA-35 micelles to discriminate between stable AAA lesions with important collagen content and aneurysms that are likely to rapidly progress and eventually rupture.

Discussion

In the current study, we demonstrated the ability of high-resolution conventional and molecular MRI to detect key anatomical features of aneurysmal progression and to identify the presence of collagen in the aneurysmal wall in a new AAA mouse model. Conventional multisequence black-blood MRI permitted the visualization of the different stages of AAA progression. Over the course of aneurysm development, we reported the accurate identification of the primary fibrotic response in the vessel wall with consequent luminal stenosis. As the aneurysm progressed, we visualized the medial rupture with blood infiltrating the remodeled adventitia, which resulted in the formation of a double channel. The ensuing increase in aortic diameter was clearly noted and quantified. Histological examination on the death of the animals matched the MR observations and confirmed the presence of the aforementioned landmarks of aneurysmal progression.

Molecular MRI, via intravenous administration of collagen-targeted CNA-35 micelles, provided valuable information about the presence of collagen in the aneurysmal wall. The injection of CNA-35 micelles resulted in a significantly higher MR signal enhancement than the injection of mutant CNA-35 micelles. Histological staining for collagen in corresponding sections confirmed the presence of collagen in the areas of MR signal enhancement. Additional examination with fluorescent confocal microscopy demonstrated the precise co-localization of CNA-35 micelles with collagen stained in the remodeled adventitia. Importantly, in a proof-of-concept experiment, CNA-35 micelle-enhanced MRI allowed the differentiation between stable AAA lesions and aneurysms that are likely to rapidly progress and rupture.

Imaging technologies in general, and ultrasound imaging in particular, are currently used to obtain information related to AAA in humans (19,20). An angiography is routinely performed to obtain preoperative anatomical information on the aneurysm and its relationship to surrounding structures (21). However, disadvantages include the use of contrast and exposure to radiation. As for ultrasound imaging, it is widely used to monitor AAA progression, but it provides little contrast and suffers from a poor signal-to-noise ratio, which limits the ability to obtain a detailed evaluation of the remodeled adventitia, particularly in preclinical studies involving small-animal models. Although some recent reports have shown the ability of ultrasound Doppler to identify medial rupture and differentiate between the lumen and the false channel in mice (5), the resolution of ultrasound remains subpar compared with MRI.

Recently, MRI has been used successfully by Turner et al. (22) to assess the development of an Ang II–induced aneurysm model in hypercholesterolemic mice. The inves-

tigators revealed that MR measurements of the AAA area performed on a bright-blood sequence were precisely correlated with the AAA area measured by using histology. In the current study, the aortic diameter measured with 3 different MR methods (T1W, T2W, and PDW) was evaluated at each imaging time point. The results showed a fast increase of the aortic diameter reaching 50% (the minimum value to define an aneurysm) 5 days after the initiation of the experiment on average. In addition to providing aortic diameter measurements, multisequence black-blood imaging offered superior contrast compared with bright-blood sequences for the examination of vessel wall remodeling during AAA formation and progression. Furthermore, it allowed the accurate identification of the medial rupture and formation of a double channel, similar to bright-blood imaging. Particularly on the T1W sequence, the medial rupture was clearly identifiable as soon as 3 days after AAA induction compared with the T2W and PDW sequences, which did not allow such evident visualization until 6 days after aneurysm initiation (Fig. 1B). In addition, multisequence black-blood imaging also offered adequate resolution to image the medial-adventitial interface. Indeed, despite various degrees of aortic stenosis caused by different degrees of collagen degradation and thrombus formation, the lumen always remained easily distinguishable from the remodeled adventitia, even on blood extravasation in the adventitial space. Multisequence black-blood MR imaging offers the benefit of increased accuracy in characterizing the anatomical features of AAA temporal progression.

One of the biological processes underlying AAA formation and progression is the degradation of the ECM, particularly collagen. Members of the matrix metalloproteinase and cysteine protease families can degrade the highly protease-resistant structures of type I and type III collagen (23–25). After the destabilization of the collagen structure, other less specific proteases can further degrade collagen. This increased collagen degradation in combination with inadequate collagen deposition has been associated with the progression and ultimately rupture of AAAs. Therefore, imaging collagen might offer additional insights about the state of aneurysm progression. CNA-35 consists of 2 N domains (N1 and N2) from a collagen adhesion protein originating from *Staphylococcus aureus* and was used as a targeting ligand. Its specificity for collagen was previously demonstrated in vitro and in vivo (9,10,12,13). In its open conformation, the CNA-35 protein can fold and lock around the collagen fiber (11). This binding process implies that CNA-35 micelles would also adhere to individual triple helical fibers of collagen, which are hardly present in healthy tissue, in addition to binding to mature collagen fibers. Degraded collagen and newly formed collagen fibers, highly present in advanced stages of AAA, are associated with high portions of free triple helices. Therefore, the bright signal enhancement observed in the aneurysmal wall of animals injected with CNA-35 micelles might derive from a combination of the micelles' increased affinity to mature collagen fibers as well as to unstructured collagen present in AAAs (7). When CNA-35 micelles were injected in animals in healthy animals, no MR signal enhancement was observed (Fig. 2B). Given the size of these particles (25 nm), their inability to penetrate healthy tissue is likely to be the limiting factor to collagen binding.

It is apparent that the degree of adventitial collagen degradation relates to the stage of aneurysmal severity. In fact, it has been shown previously that increased collagen degradation is associated with AAA progression and ultimately rupture (7). Thus, one could argue that increased level of collagen in the aortic wall stabilizes the aneurysm. We therefore hypothesized that CNA-35 micelles would allow the distinction between stable collagen-rich AAA lesions and collagen-poor lesions that are more likely to progress and rupture. To that end, we designed a proof-of-concept experiment in which the normalized signal enhancement relative to CNA-35 injection was calculated at early and late stage of AAA development and correlated with the aneurysm severity determined by their morphology (stage I to IV). Our findings revealed the ability of CNA-35 micelles to identify stable aneurysms, as the collagen-rich response of the aortic wall of noncomplicated lesions was recognizable with a high NSE percentage value (Fig. 5). In addition, a decrease of CNA-35 uptake at early stage of aneurysmal development (day 5) in stage III and IV aneurysms was associated with a rupture of the medial layer of the aorta and subsequent critical AAA progression. Interestingly, the medial rupture seemed to occur in the areas of lowest CNA-35 uptake (Fig. 5, arrow). Importantly, lesions with the lowest %NSE value that did not increase at follow-up were identified as fatal stage IV aneurysms and presented critical collagen degradation compared with viable stage III aneurysms.

Although collagen is likely not the only biological component at play in AAA progression and rupture, its precise monitoring may benefit diagnosis and staging of the aneurysm. Our results show that CNA-35 micelle-enhanced MRI represents an extremely interesting concept for the detection of collagen in the aneurysmal wall and has potential for predicting the course of AAA development. However, because of the low number of animals per group in that experiment, more extensive studies are necessary to confirm the predictive value of CNA-35 micelle-enhanced MRI in assessing AAA progression/rupture.

The current clinical guidelines (26) for the management of aneurysms are mainly based on the size of aneurysms and recommend repeated anatomical imaging every 3 to 6 months for aneurysms >4 cm. Endovascular repair or surgery is recommended for AAAs that are >5.5 cm, symptomatic, or fast growing. Intervention is not indicated when these criteria are not met as the chance of rupture is $<2.1\%$ (25). The high rate of mortality associated with reparative surgery would expose patients to unnecessary risks. Noninvasive imaging approaches, such as high-resolution multisequence black-blood MRI and collagen-targeted MRI described in this study, could ultimately improve the identification of patients at risk and facilitate the clinical management of AAAs (27). It is noteworthy that other biological targets involved in AAA

pathology are also persuaded as imaging targets in an effort to improve the characterization of the aneurysmal wall. Nahrendorf et al. (28) developed a macrophage-targeted nanoparticle for positron emission tomography–computed tomography detection of inflammation in aortic aneurysms. Recently, a pilot study used ultrasmall superparamagnetic iron oxide nanoparticles uptaken to predict aneurysm growth in humans (29). In addition, such anatomical and biological information obtained may replace the preoperative need of a computed tomography angiography.

Conclusions

We revealed that high-resolution, multisequence MRI allowed the visualization of critical features of vessel remodeling inherent to AAA formation and progression, whereas collagen-targeted nanoparticle-enhanced MRI permitted the noninvasive detection of collagen, an essential component in aneurysm pathology.

Acknowledgment
The authors acknowledge Dr. Rolando Nolasco for his work on the histological samples.

Reprint requests and correspondence to: Dr. Zahi A. Fayad, Translational and Molecular Imaging Institute, Mount Sinai School of Medicine, Atran Berg Laboratory Building, Floor 8, Room AB8-826, 1428 Madison Avenue, New York, New York 10029. E-mail: zahi.fayad@mssm.edu.

REFERENCES

1. Thompson RW, Geraghty PJ, Lee JK. Abdominal aortic aneurysms: basic mechanisms and clinical implications. Curr Probl Surg 2002;39:110–230.
2. Sakalihasan N, Limet R, Defawe OD. Abdominal aortic aneurysm. Lancet 2005;365:1577–89.
3. Michel JB. Contrasting outcomes of atheroma evolution: intimal accumulation versus medial destruction. Arterioscler Thromb Vasc Biol 2001;21:1389–92.
4. Powell JT, Brady AR. Detection, management, and prospects for the medical treatment of small abdominal aortic aneurysms. Arterioscler Thromb Vasc Biol 2004;24:241–5.
5. Wang Y, Ait-Oufella H, Herbin O, et al. TGF-beta activity protects against inflammatory aortic aneurysm progression and complications in angiotensin II-infused mice. J Clin Invest 2010;120:422–32.
6. Hellenthal FA, Buurman WA, Wodzig WK, Schurink GW. Biomarkers of abdominal aortic aneurysm progression. Part 2: inflammation. Nat Rev Cardiol 2009;6:543–52.
7. Abdul-Hussien H, Soekhoe RG, Weber E, et al. Collagen degradation in the abdominal aneurysm: a conspiracy of matrix metalloproteinase and cysteine collagenases. Am J Pathol 2007;170:809–17.
8. Mulder WJ, Griffioen AW, Strijkers GJ, Cormode DP, Nicolay K, Fayad ZA. Magnetic and fluorescent nanoparticles for multimodality imaging. Nanomedicine (Lond) 2007;2:307–24.
9. Megens RT, Oude Egbrink MG, Cleutjens JP, et al. Imaging collagen in intact viable healthy and atherosclerotic arteries using fluorescently labeled CNA35 and two-photon laser scanning microscopy. Mol Imaging 2007;6:247–60.
10. Boerboom RA, Krahn KN, Megens RT, van Zandvoort MA, Merkx M, Bouten CV. High resolution imaging of collagen organisation and synthesis using a versatile collagen specific probe. J Struct Biol 2007;159:392–99.
11. Zong Y, Xu Y, Liang X, et al. A 'Collagen Hug' model for *Staphylococcus aureus* CNA binding to collagen. EMBO J 2005;24:4224–36.
12. Helms BA, Reulen SW, Nijhuis S, de Graaf-Heuvelmans PT, Merkx M, Meijer EW. High-affinity peptide-based collagen targeting using synthetic phage mimics: from phage display to dendrimer display. J Am Chem Soc 2009;131:11683–5.
13. Sanders HM, Strijkers GJ, Mulder WJ, et al. Morphology, binding behavior and MR-properties of paramagnetic collagen-binding liposomes. Contrast Media Mol Imaging 2009;4:81–8.
14. Manning MW, Cassi LA, Huang J, et al. Abdominal aortic aneurysms: fresh insights from a novel animal model of the disease. Vasc Med 2002;7:45–54.
15. Duguet E, Vasseur S, Mornet S, Devoisselle JM. Magnetic nanoparticles and their applications in medicine. Nanomedicine (Lond) 2006;1:157–68.
16. Bulte JW. Hot spot MRI emerges from the background. Nat Biotechnol 2005;23:945–6.
17. Sosnovik DE, Nahrendorf M, Deliolanis N, et al. Fluorescence tomography and magnetic resonance imaging of myocardial macrophage infiltration in infarcted myocardium in vivo. Circulation 2007;115:1384–91.
18. Sosnovik DE, Schellenberger EA, Nahrendorf M, et al. Magnetic resonance imaging of cardiomyocyte apoptosis with a novel magneto-optical nanoparticle. Magn Reson Med 2005;54:718–24.
19. Martin-McNulty B, Vincelette J, Vergona R, Sullivan ME, Wang YX. Noninvasive measurement of abdominal aortic aneurysms in intact mice by a high-frequency ultrasound imaging system. Ultrasound Med Biol 2005;31:745–9.
20. Barisione C, Charnigo R, Howatt DA, Moorleghen JJ, Rateri DL, Daugherty A. Rapid dilation of the abdominal aorta during infusion of angiotensin II detected by noninvasive high-frequency ultrasonography. J Vasc Surg 2006;44:372–6.
21. Willmann JK, Wildermuth S, Pfammatter T, et al. Aortoiliac and renal arteries: prospective intraindividual comparison of contrast-enhanced three-dimensional MR angiography and multi-detector row CT angiography. Radiology 2003;226:798–811.
22. Turner GH, Olzinski AR, Bernard RE, et al. In vivo serial assessment of aortic aneurysm formation in apolipoprotein E-deficient mice via MRI. Circ Cardiovasc Imaging. 2008;1:220.
23. Lindholt JS, Erlandsen EJ, Henneberg EW. Cystatin C deficiency is associated with the progression of small abdominal aortic aneurysms. Br J Surg 2001;88:1472–5.
24. Lutgens SP, Cleutjens KB, Daemen MJ, Heeneman S. Cathepsin cysteine proteases in cardiovascular disease. FASEB J 2007;21:3029–41.
25. Sakalihasan N, Delvenne P, Nusgens BV, Limet R, Lapiere CM. Activated forms of MMP2 and MMP9 in abdominal aortic aneurysms. J Vasc Surg 1996;24:127–33.
26. Hirsch AT, Haskal ZJ, Hertzer NR, et al. ACC/AHA guidelines for the management of patients with peripheral arterial disease (lower extremity, renal, mesenteric, and abdominal aortic): a collaborative report from the American Associations for Vascular Surgery/Society for Vascular Surgery, Society for Cardiovascular Angiography and Interventions, Society for Vascular Medicine and Biology, Society of Interventional Radiology, and the ACC/AHA Task Force on Practice Guidelines (Writing Committee to Develop Guidelines for the Management of Patients with Peripheral Arterial Disease)—summary of recommendations. J Vasc Interv Radiol 2006;17:1383–97, quiz 1398.
27. Klink A, Hyafil F, Rudd J, et al. Diagnostic and therapeutic strategies for small abdominal aortic aneurysms. Nat Rev Cardiol 2011;8:338–47.
28. Nahrendorf M, Keliher E, Marinelli B, et al. Detection of macrophages in aortic aneurysms by nanoparticle positron emission tomography-computed tomography. Arteriosclr Thromb Vasc Biol 2011;31:750–7.
29. Richards JM, Semple SI, Macgillivray TJ, et al. Abdominal aortic aneurysm growth predicted by uptake of ultrasmall superparamagnetic particles of iron oxide: a pilot study. Circ Cardiovasc Imaging 2011;4:274–81.

Key Words: abdominal aortic aneurysm ■ collagen ■ molecular imaging ■ MRI.

APPENDIX

For supplementary materials (including tables and figures), please see the online version of this article.